Nonlinearity-induced topological phase transition characterized by the nonlinear Chern number

Kazuki Sone [1] ✉, **Motohiko Ezawa** [1], **Yuto Ashida** [2,3],
Nobuyuki Yoshioka [1,4,5] & **Takahiro Sagawa** [1,6]

As first demonstrated by the characterization of the quantum Hall effect by the Chern number, topology provides a guiding principle to realize the robust properties of condensed-matter systems immune to the existence of disorder. The bulk–boundary correspondence guarantees the emergence of gapless boundary modes in a topological system whose bulk exhibits non-zero topological invariants. Although some recent studies have suggested a possible extension of the notion of topology to nonlinear systems, the nonlinear counterpart of a topological invariant has not yet been understood. Here we propose a nonlinear extension of the Chern number based on the nonlinear eigenvalue problems in two-dimensional systems and show the existence of bulk–boundary correspondence beyond the weakly nonlinear regime. Specifically, we find nonlinearity-induced topological phase transitions, in which the existence of topological edge modes depends on the amplitude of oscillatory modes. We propose and analyse a minimal model of a nonlinear Chern insulator whose exact bulk solutions are analytically obtained. The model exhibits the amplitude dependence of the nonlinear Chern number, for which we confirm the nonlinear extension of the bulk–boundary correspondence. Thus, our result reveals the existence of genuinely nonlinear topological phases that are adiabatically disconnected from the linear regime.

Topology is utilized to realize the robust properties of materials that are immune to disorders[1,2]. A prototypical example of topological materials is the quantum Hall effect[3,4], which was discovered in a two-dimensional semiconductor under a magnetic field. In such a two-dimensional system, the Chern number characterizes the topology of the band structure and the corresponding gapless boundary modes. This bulk–boundary correspondence lies at the heart of the robustness of topological devices utilizing boundary modes. Recent studies have also explored topological phenomena in a variety of platforms, such as photonics[5], electrical circuits[6], ultracold atoms[7], fluids[8] and mechanical lattices[9].

Although band topology has been well explored in linear systems, nonlinear dynamics is ubiquitous in classical[10–15] and interacting bosonic systems[16,17]. For example, nonlinear interactions can naturally emerge in the mean-field analysis of bosonic many-body systems, such as the Gross–Pitaevskii equations. Recent research has also studied the nonlinear effects on topological edge modes[11,12,18–28] and revealed unique topological phenomena intertwined with solitons[29–35] and

[1]Department of Applied Physics, The University of Tokyo, Bunkyo-ku, Japan. [2]Department of Physics, University of Tokyo, Bunkyo-ku, Japan. [3]Institute for Physics of Intelligence, University of Tokyo, Hongo, Japan. [4]Theoretical Quantum Physics Laboratory, RIKEN Cluster for Pioneering Research (CPR), Wako-shi, Japan. [5]Japan Science and Technology Agency (JST), PRESTO, Kawaguchi, Japan. [6]Quantum-Phase Electronics Center (QPEC), The University of Tokyo, Bunkyo-ku, Japan. ✉e-mail: sone@noneq.t.u-tokyo.ac.jp
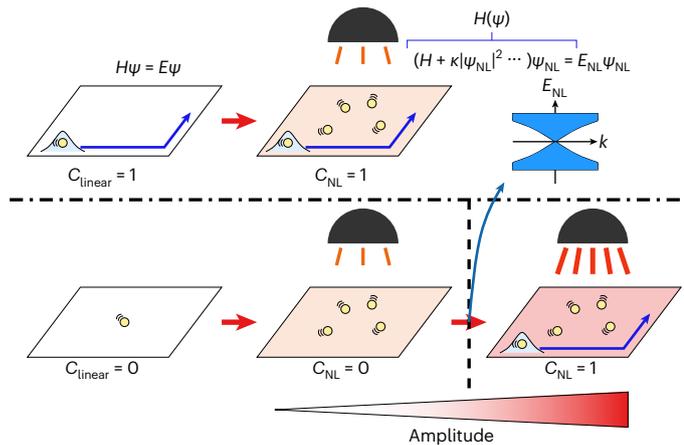
Fig. 1 | Schematic of the nonlinear Chern insulators and the nonlinearity-induced topological phase transition. Although the topology of a non-interacting linear system can be characterized by the Chern number that is computed from its eigenvectors, the topology of a nonlinear system is classified by the nonlinear Chern number, which utilizes the nonlinear extension of the eigenequation. In weakly nonlinear regions (that is, small amplitude), the nonlinear Chern number predicts the existence of edge modes corresponding to those in linear systems. Specifically, when nonlinear systems exhibit edge-localized steady states, both nonlinear and linear Chern numbers are non-zero (top). If we inject higher energy into the system and consider the eigenmodes with large amplitudes, the nonlinear band structure can become gapless. At such a gapless point, a nonlinearity-induced topological phase transition can occur, where topological boundary modes appear with the non-zero nonlinear Chern number (bottom). The nonlinearity-induced topological phases exhibit boundary modes that cannot be predicted from the linear Chern number. Therefore, such topological phases are genuinely unique to nonlinear systems.

synchronization[36–38]. Nonlinearity can further modify the conventional notion of topological phases; it has been found that one-dimensional systems can exhibit nonlinearity-induced topological phase transitions, where the existence of topological edge modes depends on the amplitude of the oscillatory modes[39–43]. Although these previous studies have indicated the existence of topological edge modes in nonlinear systems, one cannot straightforwardly extend the topological invariants to nonlinear systems because they have no band structures, at least in the conventional sense. In addition, nonlinear topology in two-dimensional systems[18,30,31,35] is much less understood than that in one-dimensional systems.

In this paper, we introduce the notion of the nonlinear Chern number and reveal its relation to the bulk–boundary correspondence. To define the nonlinear Chern number of two-dimensional systems, we consider the nonlinear extension of the eigenvalue problem[41,44] and make an analogy to band structures. Although it is not obvious that the nonlinear eigenvalue problem elucidates the bulk–boundary correspondence in nonlinear topological insulators, we theoretically prove the bulk–boundary correspondence of the nonlinear Chern number in weakly nonlinear systems. Furthermore, in stronger nonlinear regimes where nonlinear terms are larger compared with the linear bandgap, we find that the nonlinearity-induced topological phase transition can occur in two-dimensional systems (Fig. 1). We analytically show the nonlinear bulk–boundary correspondence, which states that the non-zero nonlinear Chern number predicts the existence of localized edge modes in semi-infinite systems even under strong nonlinearity. Since the nonlinearity-induced topological phases are disconnected from the linear limits under adiabatic deformations, our results show the existence of genuinely nonlinear topological phases.

The scope of this paper applies to a broad class of two-dimensional systems with $U(1)$ gauge and spatial translation symmetries, which can

be realized in a variety of experimental setups. Similar to how the Thouless–Kohmoto–Nightingale–den Nijs formula[4] triggered the research of a variety of topological materials, the nonlinear Chern number is expected to open up the research stream of nonlinear topological materials including their systematic classification. From the experiment point of view, one can realize nonlinear Chern insulators with the $U(1)$-gauge symmetry in, for example, photonics[11,12,18,20,22,24,27,30–34], ultracold atoms[16,17,27] and electrical circuits[6,36,37], where both linear band topology and nonlinear effects have been investigated. In particular, since the Kerr nonlinearity[10] is fairly common in photonic systems, it should be possible to extend the current topological photonic devices to nonlinear ones.

Nonlinear eigenvalue problem and nonlinear Chern number

We consider the nonlinear extension of the eigenvalue equations[41,43,44] and define the nonlinear Chern number by using nonlinear eigenvectors. We start from the general nonlinear dynamics:

$$i\partial_t \Psi_j(\mathbf{r}) = f_j(\mathbf{\Psi}; \mathbf{r}), \tag{1}$$

where $\Psi_j(\mathbf{r})$ is the state variable and $f_j(\cdot; \mathbf{r})$ is a nonlinear function of the state vector Ψ. In lattice systems, $\mathbf{r}$ denotes a representative point in each unit cell of the lattice (Fig. 2a). Then, j represents the internal degrees of freedom that include, for example, sublattices and effective spin degrees of freedom. When we consider continuum systems, $\mathbf{r}$ should simply represent the location and j corresponds to the internal degrees of freedom such as spins. For example, the Gross–Pitaevskii equation in the continuous space is given by $f(\Psi; \mathbf{r}) = -\nabla^2\Psi(\mathbf{r})/(2m) + V\Psi(\mathbf{r}) + (4\pi a/m)|\Psi(\mathbf{r})|^2\Psi(\mathbf{r})$, where V is a potential and m and a are the mass and scattering length, respectively. The nonlinear function $f(\cdot; \mathbf{r})$ depends on $\Psi(\mathbf{r})$ and its derivative, and has no internal degrees of freedom. Since the quantum Hall system has $U(1)$ and translation symmetries, we impose them on the nonlinear equation to study the analogy of such a prototypical topological insulator. Concretely, the $U(1)$ symmetry is represented as $f_j(e^{i\theta}\Psi; \mathbf{r}) = e^{i\theta}f_j(\Psi; \mathbf{r})$, which is satisfied in, for example, the Kerr-like nonlinearity $\kappa|\Psi_j(\mathbf{r})|^2\Psi_j(\mathbf{r})$ (ref. 10). The translational symmetry in lattice systems is defined as $f_j(\Psi; \mathbf{r} + \mathbf{a}) = f_j(\Phi; \mathbf{r})$, where $\mathbf{a}$ is a lattice vector and Φ is the translated state variable: $\Phi_j(\mathbf{r}) = \Psi_j(\mathbf{r} + \mathbf{a})$. The translational symmetry in continuum systems is also defined in the same equation, whereas $f_j(\Phi; \mathbf{r})$ still remains dependent on $\mathbf{r}$ due to, for example, the periodic potential. We also focus on conservative dynamics analogous to Hermitian Hamiltonians where the sum of squared amplitudes $\sum_{j,\mathbf{r}}|\Psi_j(\mathbf{r})|^2$ is preserved.

In accordance with the nonlinear dynamical system in equation (1), the nonlinear eigenvector and eigenvalue are defined as the state vector Ψ with components $\Psi_j(\mathbf{r})$ and the constant E that satisfy

$$f_j(\mathbf{\Psi}; \mathbf{r}) = E\Psi_j(\mathbf{r}). \tag{2}$$

We term the equation as a nonlinear eigenequation and analyse its bulk–boundary correspondence below. We note that we can regard the nonlinear eigenvector as a periodically oscillating steady state $\Psi_j(\mathbf{r}; t) = e^{-iEt}\Psi_j(\mathbf{r})$ of the nonlinear system when the eigenvalue is real. To extend the Chern number to nonlinear systems, we introduce the eigenvalue problems in the wavenumber space, which is analogous to the linear eigenequation of the Bloch Hamiltonian. In a lattice system with translation symmetries, we assume an ansatz state[41] that we name the Bloch ansatz: $\Psi_j(\mathbf{r}) = e^{i\mathbf{k}\cdot\mathbf{r}}\psi_j(\mathbf{k})$. In linear systems, the Bloch theorem guarantees that every eigenvector is given by the form of the Bloch ansatz. On the other hand, in nonlinear systems, there can be nonlinear eigenvectors out of the description of the Bloch ansatz, including bulk-localized ones. Despite the existence of such localized modes, here we only focus on nonlinear bulk eigenvectors
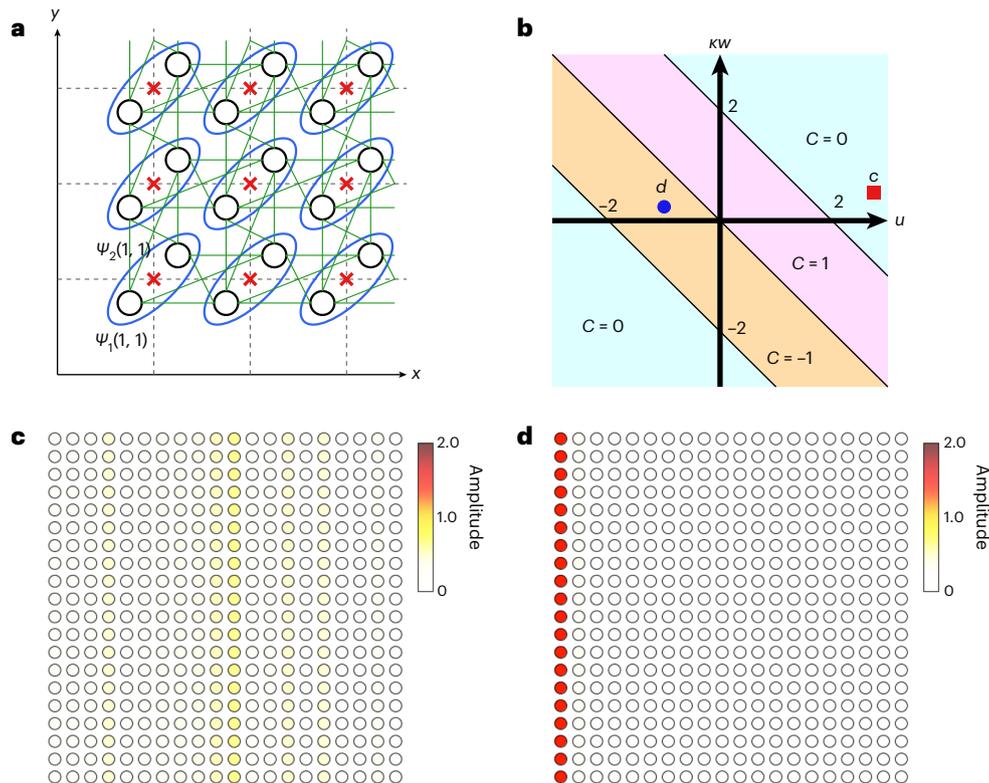
Fig. 2 | Phase diagram and dynamics of the nonlinear QWZ model.
a, Schematic of the nonlinear QWZ model. The model has two sublattices (black circles) at each lattice point encircled by the blue ellipse. The green lines represent the linear couplings. We use the notation $\Psi_i(x, y)$ to represent the state variable at each sublattice, where (x, y) is the location of the representative point of each lattice point denoted by the red cross. **b**, Analytical demonstration of the phase diagram of the nonlinear QWZ model. The horizontal axis represents the parameter of the mass term and the vertical axis corresponds to the strength of nonlinearity. The colour of each separated region represents the difference in the nonlinear Chern number. **c**, Numerical demonstration of the absence of edge modes in the topologically trivial parameter region. We simulate the dynamics of the prototypical model of a nonlinear Chern insulator starting from

an initial state localized at the left edge. We impose the open boundary condition in the x direction and the periodic boundary condition in the y direction. The figure shows the snapshot at $t = 1$. The colour shows the absolute value of the components of the state vector at each site. The parameters used are $u = 3$ and $\kappa = 0.1$, and the average amplitude is $w = 0.1$, which corresponds to the red square in **b**. **d**, Numerical demonstration of the existence of the long-lived localized state in the weakly nonlinear topological insulator. The figure shows the snapshot of the simulation at $t = 1$. The sites at the left edge show large amplitudes, which indicates the existence of the edge-localized state. The parameters used are $u = -1$ and $\kappa = 0.1$, and the average amplitude is $w = 0.1$, which corresponds to the blue circle in **b**.

described by the Bloch ansatz and show that even such periodic bulk solutions can exhibit topological phenomena inherent to nonlinear systems, namely, the nonlinearity-induced topological phase transition. Under this ansatz and $U(1)$ symmetry, one can rewrite the nonlinear eigenequation as $f_j(\mathbf{k}, \boldsymbol{\psi}(\mathbf{k})) = E(\mathbf{k})\psi_j(\mathbf{k})$ parametrized by $\mathbf{k}$ (Supplementary Note 1 provides a detailed derivation). We note that in finite periodic systems, the Bloch-ansatz solution is still an eigenvector, whereas it can be unstable under superposition with other eigenstates.

To capture the nonlinearity-induced topological phase transition depending on amplitudes, we focus on a special solution of the nonlinear eigenvector at each $\mathbf{k}$ whose sum of the squared amplitudes $\sum_j |\psi_j(\mathbf{k})|^2 = w$ is fixed independently of wavenumber $\mathbf{k}$. We note that the assumption of such fixed-amplitude Bloch-ansatz solutions is consistent with the perturbative calculation of the nonlinear eigenvectors (Methods). By using fixed-amplitude nonlinear eigenvectors, we define the nonlinear Chern number as

$$C_{\mathrm{NL}}(w) = \frac{1}{2\pi i} \int \nabla_{\mathbf{k}} \times \left(\frac{1}{\sqrt{w}} \langle \psi(\mathbf{k})| \right) \nabla_{\mathbf{k}} \left(\frac{1}{\sqrt{w}} |\psi(\mathbf{k})\rangle \right) d^2\mathbf{k}. \quad (3)$$

We note that this definition is reduced to the conventional linear Chern number if f defined in equation (2) is a linear function. It is also noteworthy that since special solutions of nonlinear eigenvectors should

exist at arbitrary w in ordinary nonlinear systems, we can define the nonlinear Chern number at any positive w except for gap-closing points. One can prove that the nonlinear Chern number is an integer by embedding the nonlinear eigenvectors into an eigenspace of a linear Bloch Hamiltonian (Supplementary Note 2). The main purpose of this paper is to show the bulk–boundary correspondence for this nonlinear Chern number. Since the eigenvector can be changed by the amplitude w, the nonlinear Chern number also depends on w (Fig. 1). Therefore, the nonlinear Chern number can predict the nonlinearity-induced topological phase transition by the change in amplitude of nonlinear systems, which is absent in linear systems[22,25,39–43]. Although here we define the nonlinear Chern number in lattice systems, we can also define that in continuum systems (Methods).

Since the parameter w is unique to nonlinear systems, it is non-trivial how to relate the amplitude w under the periodic boundary condition to that under the open boundary condition to formulate the bulk–boundary correspondence. There are two possible choices: one can equate w under the periodic boundary condition to either the average amplitude $w_{\mathrm{ave}} \equiv \sum_{\mathbf{r},j} |\Psi_j(\mathbf{r})|^2 / L$ or the edge amplitude $w_{\mathrm{edge}} \equiv \sum_j |\Psi_j(\mathbf{r}_{\mathrm{edge}})|^2$ in the model under the open boundary condition, the latter of which is used to calculate the corresponding edge modes. As shown later, both definitions can predict the topological phase transition in the continuum limit.
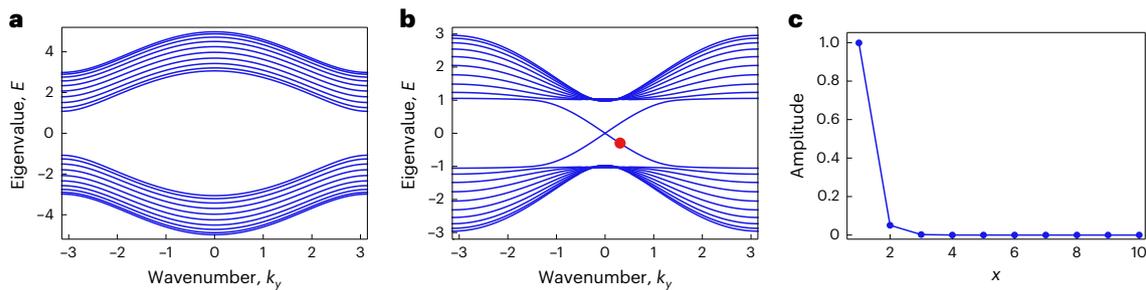
Fig. 3 | Nonlinear band structure and edge modes of the weakly nonlinear QWZ model. a, We numerically calculate the nonlinear band structure of the topologically trivial system under the open boundary condition in the x direction and the periodic boundary condition in the y direction. In the data shown in **a** and **b**, we relate the average amplitude w_{ave} to the amplitude of the bulk modes w. One can confirm the absence of gapless modes. The parameters used are $u = 3$, $\kappa = 0.1$ and $w = 0.1$. **b**, Nonlinear band structure of the topologically non-trivial system is numerically calculated. There are gapless modes that connect the upper and lower bulk bands. The parameters used are $u = -1$, $\kappa = 0.1$ and $w = 0.1$. **c**, Spatial distribution of the gapless mode is presented. The eigenvalue of the localized mode corresponds to the red circle in the band structure in **b**.

Previous research on one-dimensional nonlinear systems[43] has indicated the appearance of higher-order correction terms in the topological invariant due to multifrequency effects in nonlinear eigenvectors. However, under the $U(1)$ symmetry, higher-order terms are excluded from the nonlinear Chern number. We also note that the Bloch ansatz does not describe bulk-localized solutions that can be obtained in strongly nonlinear systems, whereas the ansatz still captures nonlinearity-induced topological phenomena. Therefore, we mainly focus on weakly and more strongly nonlinear systems where the nonlinear terms are smaller than the linear terms (Supplementary Note 3 shows the Bloch-wave-like solutions of the bulk modes in this parameter region).

Nonlinear Chern number calculated from exact solutions

To investigate the bulk–boundary correspondence, that is, the correspondence between the non-zero nonlinear Chern number and the existence of the edge-localized steady state, we propose and analyse the nonlinear extension of the Qi–Wu–Zhang (QWZ) model[45] (Methods provides the real-space description of the model). By using the Bloch ansatz, we rigorously obtain its wavenumber-space description:

$$f(\mathbf{k}, \boldsymbol{\psi}(\mathbf{k}))$$
$$= \begin{pmatrix} u + \kappa w + \cos k_x + \cos k_y & \sin k_x + i \sin k_y \\ \sin k_x - i \sin k_y & -(u + \kappa w + \cos k_x + \cos k_y) \end{pmatrix} \begin{pmatrix} \psi_1(\mathbf{k}) \\ \psi_2(\mathbf{k}) \end{pmatrix},$$
(4)

where w is the squared amplitude $w = |\psi_1(\mathbf{k})|^2 + |\psi_2(\mathbf{k})|^2$; u and κ are dimensionless parameters of the linear and nonlinear mass terms, respectively. Here we introduce the staggered Kerr-like nonlinearity $\pm \kappa w$ to the linear Chern insulator model[45].

To calculate the nonlinear Chern number, we focus on special solutions where the squared amplitude w is fixed independent of wavenumber $\mathbf{k}$. Then, we can regard equation (4) as a linear equation and thus can analytically obtain the exact bulk solutions of the nonlinear eigenvalues and eigenvectors as the linear QWZ model. Using the exactly obtained nonlinear eigenvectors, we calculate the nonlinear Chern number and obtain the phase diagram shown in Fig. 2b (Methods shows the detailed calculation and Supplementary Note 6 provides the numerical confirmation). The amplitude dependence of the nonlinear Chern number indicates the existence of the nonlinearity-induced topological phase transition in the nonlinear QWZ model. We note that since we calculate the nonlinear Chern number from the exact nonlinear eigenvectors, our result shows the

existence of the nonlinearity-induced topological phase transition without any approximations. Such an analytical demonstration of the nonlinearity-induced topological phase transition is achieved by considering nonlinear equations with the form

$$i\partial_t \psi_n(\mathbf{k}; t) = \sum_m f_{nm} \left(\sum_j |\psi_j(\mathbf{k}; t)|^2 \right) \psi_m(\mathbf{k}; t),$$
(5)

where ψ_j and $\mathbf{k}$ are the state variables and wavenumber, respectively. Under the existence of a more general nonlinear term, we may also define and calculate the nonlinear Chern number by appropriately defining w (Supplementary Notes 4 and 5).

Bulk–boundary correspondence in weakly nonlinear systems

We first numerically confirm the bulk–boundary correspondence in weakly nonlinear systems. We simulate the dynamics of the nonlinear QWZ model (equation (4)) with weak nonlinearity, where the nonlinear Chern number is the same as that in the linear limit $\kappa w \to 0$. In the topological phase ($C_{NL} = \pm 1$; Fig. 2d), we find a long-lived localized state that corresponds to a topological edge mode in the QWZ model. Meanwhile, in the case of $C_{NL} = 0$ (Fig. 2c), the edge-localized initial state is spread to the bulk, which indicates the absence of edge modes. We also confirm the bulk–boundary correspondence from the perspective of the nonlinear band structure (Fig. 3; Methods provides the numerical method), which implies the utility of the nonlinear band structure to detect topological edge modes.

In fact, the bulk–boundary correspondence between the nonlinear Chern number and the gapless edge modes can be established in general weakly nonlinear systems. We mathematically show the bulk–boundary correspondence under weak nonlinearity compared with the linear bandgap. Methods and Supplementary Note 7 describe the details of the theorem and its proof.

Nonlinearity-induced topological phase transition

We next show that nonlinearity-induced topological phase transitions occur in the stronger nonlinear regime, where the nonlinear Chern number becomes nonzero and topological edge modes appear at a critical amplitude. First, we consider continuum systems and analytically show such nonlinearity-induced topological phase transitions and the bulk–boundary correspondence under stronger nonlinearity. Specifically, we derive the effective theory of the low-energy dispersion of the nonlinear QWZ model as

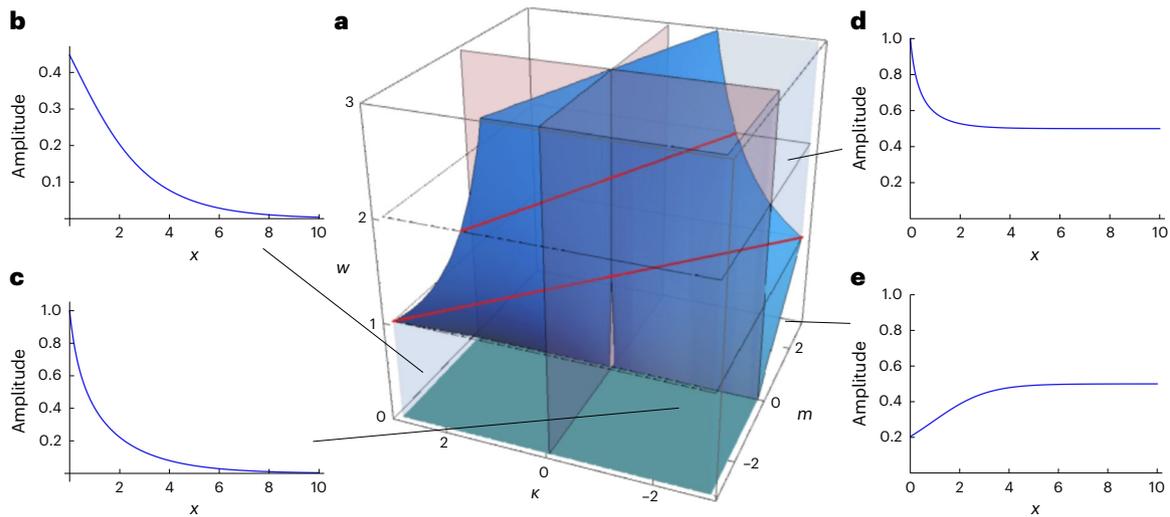$$i\partial_t \mathbf{\Psi}(\mathbf{r}) = \hat{H}(\mathbf{\Psi}(\mathbf{r}))\mathbf{\Psi}(\mathbf{r}),$$
(6)

Fig. 4 | Phase diagram and localized modes of the nonlinear Dirac Hamiltonian. a, Phase diagram of the nonlinear Dirac Hamiltonian, which demonstrates the nonlinear bulk–boundary correspondence in the continuum model. The vertical axis represents the amplitude, and the horizontal axes correspond to the parameters of the nonlinear Dirac Hamiltonian. The blue curved surface shows the phase boundary that separates a trivial phase without boundary modes and a topological phase exhibiting localized modes at the left boundary. The red surfaces present the boundaries where the sign of the parameters of the Dirac Hamiltonian changes. The red lines show the phase boundaries at the surfaces of $w = 1$ and $w = 2$. In the linear limit ($w = 0$), the topological phases are separated by the $m = 0$ axis, whereas the nonlinearity modifies the boundary of the topological phases. **b–d**, Representative shape of the localized mode in each of the topologically non-trivial parameter regions.

b, When m is negative and κ is positive, we obtain a localized mode in the small-amplitude region, which is regarded as a counterpart of a conventional topological edge mode. We set m, κ and D as $m = -0.5$, $\kappa = 1$ and $D = 3$. **c**, When both m and κ are negative, a localized mode appears independent of the amplitude as in linear topological insulators. We set $m = -0.5$, $\kappa = -1$ and $D = 3$. **d**, When m is positive and κ is negative, the nonlinear Dirac Hamiltonian exhibits the nonlinearity-induced topological phase transition. We obtain an unconventional localized mode if the amplitude is larger than a critical value. In this localized mode, there exist non-vanishing amplitudes even in the limit of $x \to \infty$. We set $m = 0.5$, $\kappa = -2$ and $D = -3$. **e**, We can also obtain anti-localized modes in the topologically trivial phase, which are unique to nonlinear systems. We set $m = 0.5$, $\kappa = -2$ and $D = -20$.

$$\hat{H}(\mathbf{\Psi}(\mathbf{r})) =$$
$$\begin{pmatrix} m + \kappa \left(|\Psi_1(\mathbf{r})|^2 + |\Psi_2(\mathbf{r})|^2 \right) & -\mathrm{i}\partial_x + \partial_y \\ -\mathrm{i}\partial_x - \partial_y & -m - \kappa \left(|\Psi_1(\mathbf{r})|^2 + |\Psi_2(\mathbf{r})|^2 \right) \end{pmatrix}, \quad (7)$$

where $m = u + 2$ and $\mathbf{\Psi}(x, y) = (\Psi_1(x, y), \Psi_2(x, y))^\mathsf{T}$ is the state-vector function at location (x, y) (Methods and Supplementary Note 8 provide the derivation). This state-dependent Hamiltonian has a similar structure to the Dirac Hamiltonian, except for the nonlinear mass term $\kappa(|\Psi_1|^2 + |\Psi_2|^2)$, and thus, we term it the nonlinear Dirac Hamiltonian. In general, the nonlinear Dirac Hamiltonian should describe the low-energy dispersions of a broad class of nonlinear topological insulators, and thus, its localized modes unveil the existence of topological edge modes in various continuum systems. By considering the right semi-infinite system which has an open boundary at $x = 0$ and are periodic in the y direction, and assuming the ansatz $(\Psi_1(x, y), \Psi_2(x, y))^\mathsf{T} = \mathrm{e}^{\mathrm{i}k_y y}\phi(x)(1/\sqrt{2}, -\mathrm{i}/\sqrt{2})$ $(E = k_y)$, we can analytically obtain the spatial distribution of the gapless mode of the nonlinear Dirac Hamiltonian as

$$(\Psi_1(x, y), \Psi_2(x, y))^\mathsf{T}$$
$$= \mathrm{e}^{\mathrm{i}(k_y y + \theta)} \sqrt{\frac{1}{-(\kappa/m) + D\mathrm{e}^{-2mx}}} (1/\sqrt{2}, -\mathrm{i}/\sqrt{2})^\mathsf{T}, \quad (8)$$

where D is the integral constant and $-(\kappa/m) + D\mathrm{e}^{-2mx}$ must be positive.

Figure 4 summarizes the nonlinear Chern numbers (Methods) and the behaviours of gapless modes in the nonlinear Dirac Hamiltonian at different parameters. In the case of $m < 0$, where the Chern number is $C = 1/2$ in the linear limit, we obtain the localized states at the left side as in the linear case. These localized states are consistent with the bulk–boundary correspondence in weakly nonlinear systems, as shown

earlier. We can also check that no localized modes appear in the case of positive m and κ, where the nonlinear Chern number is $C_{\mathrm{NL}} = -1/2$ at any amplitude.

To discuss the bulk–boundary correspondence under stronger nonlinearity, we must relate the amplitude w under the periodic boundary condition to $w_{\mathrm{ave}} = \int_0^L \mathrm{d}x |\phi(x)|^2 / L$ or $w_{\mathrm{edge}} = |\phi(0)|^2$ of the edge-localized mode obtained under the open boundary condition. In fact, either choice can exactly predict the phase boundary as shown in the case of $m > 0$, $\kappa < 0$, where we obtain the localized state with the residual amplitude $\sqrt{|m/\kappa|}$ in the limit of $x \to \infty$. In this case, we obtain a gapless homogeneous mode $\phi(x) = \sqrt{|m/\kappa|}$ at the phase boundary. Since both w_{ave} and w_{edge} of such a homogeneous mode are $w_{\mathrm{ave/edge}} = \sqrt{|m/\kappa|}$ and satisfy $m + \kappa w_{\mathrm{ave/edge}} = 0$, both definitions of the amplitude predict the nonlinearity-induced topological phase transition associated with the amplitude-dependent Chern number (Supplementary Note 9). We note that the non-vanishing amplitude in the limit of $x \to \infty$ indicates that it is impossible to normalize the edge mode. In finite systems, however, such a non-vanishing localized mode can be normalized and thus can robustly emerge. We also obtain anti-localized modes satisfying $|\phi(0)| < |\phi(x)|$ for $D > 0$ (Fig. 4e), which is unique to nonlinear systems.

We can also confirm the bulk–boundary correspondence in lattice systems (Supplementary Notes 10 and 12–17). Specifically, by making the correspondence between the bulk amplitude w and edge amplitude w_{edge}, the non-zero nonlinear Chern number corresponds to the existence of localized zero modes. We analytically show such bulk–boundary correspondence in semi-infinite systems and numerically confirm it in finite systems of the nonlinear QWZ model.

Observation protocol of edge modes via quench dynamics

One can observe the topological properties via quench dynamics, which directly detects the existence of topological edge modes. In quench
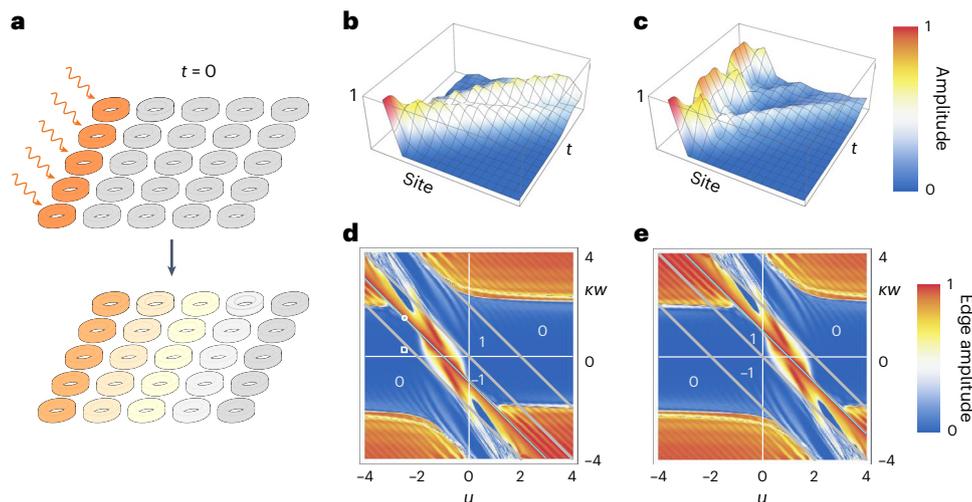
Fig. 5 | Phase diagram of the quench dynamics of the nonlinear QWZ model. **a**, Schematic of the experimental protocol of the quench dynamics. First, one excites the edge sites by, for example, applying lasers to the edge resonators in nonlinear topological photonic insulators. Then, one observes the nonlinear dynamics without external fields and confirms the existence or absence of a long-lived localized state. **b**, Time evolution of the quench dynamics in a trivial phase. We use the parameters $u = -2.5$ and $\kappa = 0.25$, and set the initial edge amplitude as $w = 1$, which corresponds to the white square in **d**. We confirm the absence of localized edge modes. **c**, Time evolution of the quench dynamics of nonlinear edge modes. We use the parameters $u = -2.5$ and $\kappa = 1.5$, and set the initial edge amplitude as $w = 1$, which corresponds to the white circle in **d**. We confirm that a localized state remains for a long time, which indicates the existence of edge

modes. **d,e**, Simulation of the quench dynamics and a plot of the amplitude remaining at the edge sites in the long-term limit after a quench in the u–κw plane. The light-blue lines indicate the parameters where we can obtain the exact edge-localized solutions. The white numbers show the nonlinear Chern number, and the grey lines represent their phase boundaries, where we relate the amplitude w to $w_{\text{edge}} = \sum_j |\Psi_j(x = 0)|^2$ at $t = 0$. These lines agree with the boundary of the topological phase, and thus, the quench dynamics shows the shift in the phase boundary by nonlinearity. We take the different initial configurations corresponding to the edge modes in the linear limit at $u = -1$ in **d** and $u = 1$ in **e**. Thus, the phase diagrams of the quench dynamics reproduce the topological phases with different Chern numbers in these panels ($C = -1$ for **d** and $C = 1$ for **e**).

dynamics, one only has to excite the edge sites at homogeneous amplitudes and observe the dynamics without any other external interactions (Fig. 5a). To confirm the correspondence between the existence of nonlinear edge modes and the localized states in quench dynamics, we numerically simulate the quench dynamics of a nonlinear QWZ model (equation (4)) at various parameters. Figure 5b,c shows the time evolution of the quench dynamics with and without nonlinear edge modes. We also obtain the phase diagrams (Fig. 5d,e), which are classified by the amplitude at the edge of the sample in the long-time limit. Here we consider two initial states equivalent to the nonlinear edge modes at $u + \kappa w = \pm 1$ (Methods). We confirm that the localized states remain in the topological cases and vanish in the trivial cases. Identifying the bulk amplitude w as $w_{\text{edge}} = \sum_{j,y} |\Psi_j(0, y)|^2 / L_y$ (L_y is the system size in the y direction) of the initial state, we confirm that the nonlinear Chern number $C_{\text{NL}}(w)$ roughly corresponds to the phase boundaries in the quench dynamics, which indicates that the nonlinear Chern number and its nonlinearity-induced topological phase transition can predict the existence of experimentally observable localized states.

Possible experimental setups of nonlinear Chern insulators

Nonlinear Chern insulators are expected to be realized by using topological photonics with the Kerr nonlinearity. In particular, we can replace the nonlinear term in equation (4) by on-site Kerr nonlinear terms, that is, $\kappa |\Psi_j(x, y)|^2 \Psi_j(x, y)$, and such Kerr nonlinearity is feasible in various photonic systems. Supplementary Note 18 further discusses a possible optical setup and the analytical demonstration of the nonlinearity-induced topological phase transition under the on-site Kerr nonlinearity.

Discussions

Our results indicate the existence of unique topological phenomena beyond the weakly nonlinear regime. There remain intriguing issues to

establish the topological classification of nonlinear systems including further strongly nonlinear cases where nonlinearity is even stronger than the linear couplings. Since such strong nonlinearity can induce bulk-localized modes[18,35,42,46] and topological edge solitons[30–35] that are out of the description of the Bloch ansatz, it is unclear whether or not the nonlinear Chern number still fully works. We can also discuss the linear stability of the Bloch-ansatz state, which may be related to the topological phase transition[28] (Supplementary Note 19). It may also be intriguing to investigate the connection to many-body quantum physics because nonlinear terms can be derived from the mean-field approximation[16,17] or the Kohn–Sham equation[47,48] of interacting systems in general (Supplementary Note 20). Therefore, the nonlinear topology may also be useful to understand the topology of interacting systems.

Online content

Any methods, additional references, Nature Portfolio reporting summaries, source data, extended data, supplementary information, acknowledgements, peer review information; details of author contributions and competing interests; and statements of data and code availability are available at https://doi.org/10.1038/s41567-024-02451-x.

References

1. Kane, C. L. & Mele, E. J. Z_2 topological order and the quantum spin Hall effect. *Phys. Rev. Lett.* **95**, 146802 (2005).
2. Hazan, M. Z. & Kane, C. L. Colloquium: topological insulators. *Rev. Mod. Phys.* **82**, 3045–3067 (2010).
3. Klitzing, K. V., Dorda, G. & Pepper, M. New method for high-accuracy determination of the fine-structure constant based on quantized Hall resistance. *Phys. Rev. Lett.* **45**, 494–497 (1980).
4. Thouless, D. J., Kohmoto, M., Nightingale, M. P. & Nijs, M. D. Quantized Hall conductance in a two-dimensional periodic potential. *Phys. Rev. Lett.* **49**, 405–408 (1982).

5. Lu, L., Joannopoulos, J. D. & Soljačić, M. Topological photonics. *Nat. Photon.* **8**, 821–829 (2014).
6. Ningyuan, J., Owens, C., Sommer, A., Schuster, D. & Simon, J. Time- and site-resolved dynamics in a topological circuit. *Phys. Rev. X* **5**, 021031 (2015).
7. Jotzu, G. et al. Experimental realization of the topological Haldane model with ultracold fermions. *Nature* **515**, 237–240 (2014).
8. Yang, Z. et al. Topological acoustics. *Phys. Rev. Lett.* **114**, 114301 (2015).
9. Kane, C. L. & Lubensky, T. C. Topological boundary modes in isostatic lattices. *Nat. Phys.* **10**, 39–45 (2013).
10. Boyd, R. W. *Nonlinear Optics* (Academic Press, 2003).
11. Smirnova, D., Leykam, D., Chong, Y. & Kivshar, Y. Nonlinear topological photonics. *Appl. Phys. Rev.* **7**, 021306 (2020).
12. Ota, Y. et al. Active topological photonics. *Nanophotonics* **9**, 547–567 (2020).
13. Acebrón, J. A., Bonilla, L. L., Pérez, V. C. J., Ritort, F. & Spigler, R. The Kuramoto model: a simple paradigm for synchronization phenomena. *Rev. Mod. Phys.* **77**, 137–185 (2005).
14. Strogatz, S. H. *Nonlinear Dynamics and Chaos with Student Solutions Manual: With Applications to Physics, Biology, Chemistry, and Engineering* (CRC Press, 2018).
15. Marchetti, M. C. et al. Hydrodynamics of soft active matter. *Rev. Mod. Phys.* **85**, 1143–1189 (2013).
16. Gross, E. P. Structure of a quantized vortex in boson systems. *Nuovo Cim.* **20**, 454–477 (1961).
17. Pitaevskii, L. P. Vortex lines in an imperfect Bose gas. *Sov. Phys. JETP* **13**, 451–454 (1961).
18. Lumer, Y., Plotnik, Y., Rechtsman, M. C. & Segev, M. Self-localized states in photonic topological insulators. *Phys. Rev. Lett.* **111**, 243905 (2013).
19. Bomantara, R. W., Zhao, W., Zhou, L. & Gong, J. Nonlinear Dirac cones. *Phys. Rev. B* **96**, 121406 (2017).
20. Harari, G. et al. Topological insulator laser: theory. *Science* **359**, 1230 (2018).
21. Zangeneh-Nejad, F. & Fleury, R. Nonlinear second-order topological insulators. *Phys. Rev. Lett.* **123**, 053902 (2019).
22. Maczewsky, L. J. et al. Nonlinearity-induced photonic topological insulator. *Science* **370**, 701–704 (2020).
23. Lo, P. W. et al. Topology in nonlinear mechanical systems. *Phys. Rev. Lett.* **127**, 076802 (2021).
24. Jürgensen, M., Mukherjee, S. & Rechtsman, M. C. Quantized nonlinear Thouless pumping. *Nature* **596**, 63–67 (2021).
25. Mochizuki, K., Mizuta, K. & Kawakami, N. Fate of topological edge states in disordered periodically driven nonlinear systems. *Phys. Rev. Research* **3**, 043112 (2021).
26. Fu, Q., Wang, P., Kartashov, Y. V., Konotop, V. V. & Ye, F. Nonlinear Thouless pumping: solitons and transport breakdown. *Phys. Rev. Lett.* **128**, 154101 (2022).
27. Mostaan, N., Grusdt, F. & Goldman, N. Quantized topological pumping of solitons in nonlinear photonics and ultracold atomic mixtures. *Nat. Commun.* **13**, 5997 (2022).
28. Leykam, D., Smolina, E., Maluckov, A., Flach, S. & Smirnova, D. A. Probing band topology using modulational instability. *Phys. Rev. Lett.* **126**, 073901 (2021).
29. Chen, B. G., Upadhyaya, N. & Vitelli, V. Nonlinear conduction via solitons in a topological mechanical insulator. *Proc. Natl Acad. Sci. USA* **111**, 13004–13009 (2014).
30. Leykam, D. & Chong, Y. D. Edge solitons in nonlinear-photonic topological insulators. *Phys. Rev. Lett.* **117**, 143901 (2016).
31. Zhang, Z. et al. Observation of edge solitons in photonic graphene. *Nat. Commun.* **11**, 1902 (2020).
32. Ivanov, S. K., Kartashov, Y. V., Maczewsky, L. J., Szameit, A. & Konotop, V. V. Edge solitons in Lieb topological Floquet insulator. *Opt. Lett.* **45**, 1459–1462 (2020).
33. Mukherjee, S. & Rechtsman, M. C. Observation of unidirectional solitonlike edge states in nonlinear Floquet topological insulators. *Phys. Rev. X* **11**, 041057 (2021).
34. Li, R. et al. Topological bulk solitons in a nonlinear photonic Chern insulator. *Commun. Phys.* **5**, 275 (2022).
35. Ezawa, M. Nonlinearity-induced chiral solitonlike edge states in Chern systems. *Phys. Rev. B* **106**, 195423 (2022).
36. Kotwal, T. et al. Active topolectrical circuits. *Proc. Natl Acad. Sci. USA* **118**, e2106411118 (2021).
37. Sone, K., Ashida, Y. & Sagawa, T. Topological synchronization of coupled nonlinear oscillators. *Phys. Rev. Research* **4**, 023211 (2022).
38. Wächtler, C. W. & Platero, G. Topological synchronization of quantum van der Pol oscillators. *Phys. Rev. Research* **5**, 023021 (2023).
39. Hadad, Y., Khanikaev, A. B. & Alù, A. Self-induced topological transitions and edge states supported by nonlinear staggered potentials. *Phys. Rev. B* **93**, 155112 (2016).
40. Darabi, A. & Leamy, M. J. Tunable nonlinear topological insulator for acoustic waves. *Phys. Rev. Appl.* **12**, 044030 (2019).
41. Tuloup, T., Bomantara, R. W., Lee, C. H. & Gong, J. Nonlinearity induced topological physics in momentum space and real space. *Phys. Rev. B* **102**, 115411 (2020).
42. Ezawa, M. Nonlinearity-induced transition in the nonlinear Su-Schrieffer-Heeger model and a nonlinear higher-order topological system. *Phys. Rev. B* **104**, 235420 (2021).
43. Zhou, D., Rocklin, D. Z., Leamy, M. & Yao, Y. Topological invariant and anomalous edge modes of strongly nonlinear systems. *Nat. Commun.* **13**, 3379 (2022).
44. Li, F., Wang, J., Cui, D., Xue, K. & Yi, X. X. Bloch band structures and linear response theory of nonlinear systems. *Int. J. Mod. Phys. B* **0**, 2450322 (2023).
45. Qi, X. L., Wu, Y. S. & Zhang, S. C. Topological quantization of the spin Hall effect in two-dimensional paramagnetic semiconductors. *Phys. Rev. B* **74**, 085308 (2006).
46. Eilbeck, J. C., Lomdahl, P. S. & Scott, A. C. The discrete self-trapping equation. *Phys. D* **16**, 318–338 (1985).
47. Strandberg, T. O., Canali, C. M. & MacDonald, A. H. Calculation of Chern number spin Hamiltonians for magnetic nano-clusters by DFT methods. *Phys. Rev. B* **77**, 174416 (2008).
48. Dongbin, S. et al. Unraveling materials Berry curvature and Chern numbers from real-time evolution of Bloch states. *Proc. Natl Acad. Sci. USA* **116**, 4135–4140 (2019).

Methods

Justification of the Bloch ansatz via perturbation analysis

If the nonlinear term is small compared with the linear bandgap, one can regard the nonlinear effect as a perturbation to the linear band structure. Under such an assumption, one can perturbatively calculate the nonlinear eigenvectors. To show the perturbation calculation protocol of the nonlinear eigenvalue problem, we rewrite the nonlinear eigenequation as

$$H(\mathbf{\Psi})\mathbf{\Psi} = (H^0 + \kappa H_{NL}(\mathbf{\Psi}))\mathbf{\Psi} = E\mathbf{\Psi}. \tag{9}$$

We consider the perturbation expansion by κ as follows:

$$\mathbf{\Psi} = \mathbf{\Psi}^{(0)} + \kappa\mathbf{\Psi}^{(1)} + \cdots, \tag{10}$$

$$E = E^{(0)} + \kappa E^{(1)} + \cdots. \tag{11}$$

One can determine $\mathbf{\Psi}^{(0)}$ and $E^{(0)}$ from the eigenvalue and eigenvector of the linear Hamiltonian H^0 as

$$H^0\mathbf{\Psi}^{(0)} = E\mathbf{\Psi}^{(0)}. \tag{12}$$

Then, the first-order perturbation is calculated from the eigenequation of $(H^0 + \kappa H_{NL}(\mathbf{\Psi}^{(0)}))$ as

$$\left(H^0 + \kappa H_{NL}(\mathbf{\Psi}^{(0)})\right)\left(\mathbf{\Psi}^{(0)} + \kappa\mathbf{\Psi}^{(1)}\right) = \left(E^{(0)} + \kappa E^{(1)}\right)\left(\mathbf{\Psi}^{(0)} + \kappa\mathbf{\Psi}^{(1)}\right). \tag{13}$$

One can confirm the consistency between equations (9) and (13) by substituting equations (10) and (11) into the former equation.

In translation-invariant systems, the non-perturbed eigenvector $\mathbf{\Psi}^{(0)}$ is described by a Bloch wave $\mathbf{\Psi}^{(0)} = e^{i\mathbf{k}\cdot\mathbf{x}}\mathbf{\psi}^{(0)}$, due to the Bloch theorem of linear systems. Since the Bloch wave exhibits no site dependence of the amplitude, one can assume that the nonlinear term $\kappa H_{NL}(\mathbf{\Psi})$ is also uniform, and thus, the whole effective Hamiltonian $H^0 + \kappa H_{NL}(\mathbf{\Psi})$ still has translational symmetry. Therefore, in weakly nonlinear systems, one can believe that all of the nonlinear eigenvectors are described by the Bloch ansatz. We note that in strongly nonlinear regimes, there can be localized modes that cannot be described by the Bloch ansatz[35,42,46]. However, the periodic solutions obtained from the Bloch ansatz are still exact nonlinear eigenvectors under the periodic boundary conditions.

Nonlinear Chern number in continuum systems

In continuum systems with a periodic potential, the Bloch ansatz should read $\Psi_j(\mathbf{r}) = e^{i\mathbf{k}\cdot\mathbf{r}}\psi_j(\mathbf{k}, \mathbf{r})$, where $\psi_j(\mathbf{k}, \mathbf{r})$ is a periodic function of $\mathbf{r}$ whose period is equal to that of the periodic potential. Then, the wavenumber-space representation of the nonlinear eigenequation becomes $f_j(\mathbf{k}, \mathbf{\psi}(\mathbf{k}); \mathbf{r}) = E(\mathbf{k})\psi_j(\mathbf{k}, \mathbf{r})$, and the nonlinear Chern number can be written as

$$C_{NL} = \frac{1}{2\pi i}\sum_j \int_S d^2\mathbf{r} \int \nabla_{\mathbf{k}} \times \left[(\psi_j(\mathbf{k}, \mathbf{r})/\sqrt{w})\nabla_{\mathbf{k}}(\psi_j(\mathbf{k}, \mathbf{r})/\sqrt{w})\right] d^2\mathbf{k}, \tag{14}$$

where S represents the unit cell of the periodic system. The squared amplitude is defined as $w = \sum_j\int_S d^2\mathbf{r}|\psi_j(\mathbf{k}, \mathbf{r})|^2$ in this continuum case.

Real-space description of the nonlinear QWZ model

To investigate the existence or absence of topological edge modes in lattice systems, we construct a minimal lattice model of a nonlinear Chern insulator, which we term the nonlinear QWZ model (equation (4) shows the wavenumber-space description). Its real-space dynamics is described as

$$i\frac{d}{dt}\Psi_j(x, y) = \sum_l \left\{ (\sigma_z)_{jl}\left[2u\Psi_l(x, y) + \Psi_l(x+1, y) + \Psi_l(x-1, y)\right.\right.$$
$$\left.+ \Psi_l(x, y+1) + \Psi_l(x, y-1)\right]/2$$
$$+ (\sigma_x)_{jl}\left(\Psi_l(x+1, y) - \Psi_l(x-1, y)\right)/2i$$
$$+ (\sigma_y)_{jl}\left(\Psi_l(x, y+1) - \Psi_l(x, y-1)\right)/2i\right\}$$
$$- (-1)^j\kappa\left(|\Psi_1(x, y)|^2 + |\Psi_2(x, y)|^2\right)\Psi_j(x, y), \tag{15}$$

where (j, l) and (x, y) represent the internal degree of freedom and location, respectively, and $\Psi_j(x, y)$ is the jth component of the state vector at location (x, y). The values of $(\sigma_i)_{jl}$ are the (j, l)th component of the ith Pauli matrix. This lattice model introduces the staggered Kerr-like nonlinearity $-(-1)^j\kappa(|\Psi_1(x, y)|^2 + |\Psi_2(x, y)|^2)\Psi_i(x, y)$ to the linear QWZ model[45].

Exact bulk solutions of the nonlinear QWZ model

To obtain the phase diagram shown in Fig. 2b, we analytically solve the nonlinear eigenequation in equation (4). If we focus on special solutions where the squared amplitude $|\psi_1(\mathbf{k})|^2 + |\psi_2(\mathbf{k})|^2 = w$ has no $\mathbf{k}$ dependence, the nonlinear eigenequation (equation (4)) exactly corresponds to a linear one. Therefore, by solving the corresponding linear eigenequation, we obtain the following exact bulk eigenvalues and eigenvectors as

$$E_\pm(k_x, k_y)$$
$$= \pm\sqrt{2\cos k_x \cos k_y + 2(u + \kappa w)(\cos k_x + \cos k_y) + (u + \kappa w)^2 + 2}, \tag{16}$$

$$\begin{pmatrix}\psi_{1\pm}(\mathbf{k}) \\ \psi_{2\pm}(\mathbf{k})\end{pmatrix} = \frac{\sqrt{w}}{c_\pm(\mathbf{k})}\begin{pmatrix}u + \kappa w + \cos k_x + \cos k_y + E_\pm(k_x, k_y) \\ \sin k_x - i\sin k_y\end{pmatrix}, \tag{17}$$

where $c_\pm(\mathbf{k}) = \sqrt{\left(u + \kappa w + \cos k_x + \cos k_y + E_\pm(k_x, k_y)\right)^2 + \sin^2 k_x + \sin^2 k_y}$ is a normalization constant. By using these nonlinear eigenvectors, we analytically obtain the nonlinear Chern number as

$$C_{NL} = \begin{cases} 1 & (0 < u + \kappa w < 2) \\ -1 & (-2 < u + \kappa w < 0) \\ 0 & (\text{otherwise}) \end{cases}, \tag{18}$$

as summarized in Fig. 2b. We note that one can generally obtain exact bulk solutions if the nonlinear equation has the form in equation (5) (Supplementary Note 4).

Perturbation analysis of the bulk modes of the nonlinear QWZ model

Although we calculate the exact solutions of the bulk modes of the nonlinear QWZ model in the main text, we can also obtain the same bulk modes from the perturbation analysis or self-consistent calculations. Specifically, if we conduct the perturbation analysis described earlier, the calculation stops at the first-order perturbation and derives the same bulk modes as the exact solutions.

The zeroth-order solutions, that is, the linear solutions of the bulk modes of the QWZ model are

$$\begin{pmatrix}\psi_{1\pm}^{(0)}(\mathbf{k}) \\ \psi_{2\pm}^{(0)}(\mathbf{k})\end{pmatrix} = \frac{\sqrt{w}}{c_\pm(\mathbf{k})}\begin{pmatrix}u + \cos k_x + \cos k_y + E_\pm(k_x, k_y) \\ \sin k_x - i\sin k_y\end{pmatrix}, \tag{19}$$

$$E_\pm(k_x, k_y) = \pm\sqrt{2\cos k_x \cos k_y + 2u(\cos k_x + \cos k_y) + u^2 + 2}, \tag{20}$$

$$c_\pm(\mathbf{k}) = \sqrt{\left(u + \cos k_x + \cos k_y + E_\pm(k_x, k_y)\right)^2 + \sin^2 k_x + \sin^2 k_y}, \tag{21}$$

where we fix the norm as $|\psi_{1\pm}(\mathbf{k})|^2 + |\psi_{2\pm}(\mathbf{k})|^2 = w$. Then, substituting these solutions into the state-dependent Hamiltonian of the nonlinear QWZ model, one can obtain the first-order perturbation solutions. Due to the nonlinear terms depending only on the norm of the nonlinear eigenvector, the substituted effective Hamiltonian is described as

$$H(\mathbf{k}, \mathbf{\psi}(\mathbf{k})) =$$
$$\begin{pmatrix}u + \kappa w + \cos k_x + \cos k_y & \sin k_x + i\sin k_y \\ \sin k_x - i\sin k_y & -(u + \kappa w + \cos k_x + \cos k_y)\end{pmatrix}, \tag{22}$$

independently of the wavenumber. The eigenvalues and eigenvectors of this Hamiltonian are the same as those of the nonlinear QWZ model (equations (16) and (17)), and thus, the first-order perturbation calculation is consistent with the exact solutions.

The self-consistent calculation is equivalent to the higher-order perturbation calculation (as shown later). However, if one substitutes the first-order solutions into the state-dependent Hamiltonian of the nonlinear QWZ model, one obtains the same effective Hamiltonian as equation (22). Therefore, the nonlinear eigenvectors and eigenvalues obtained from the self-consistent calculation are the same as those obtained from the first-order perturbation and exact solutions.

Numerical simulations of the real-space dynamics of the nonlinear QWZ model

In Fig. 2, we numerically calculate the dynamics of the nonlinear QWZ model by using the fourth-order Runge–Kutta method. We consider a 20×20 square lattice, where each lattice point has two internal degrees of freedom. We impose the open boundary condition in the x direction and the periodic boundary condition in the y direction. We set the time step $dt = 0.005$. The simulation starts from the localized initial states that have non-zero values $\Psi_1(x, y) = w/\sqrt{2}$ and $\Psi_2(x, y) = iw/\sqrt{2}$ only at $x = 1$. We use the parameters $u = 3$ and $\kappa = 0.1$ in Fig. 2c and $u = -1$ and $\kappa = 0.1$ in Fig. 2d. We also set the initial amplitude at the edge site as $w = 1$. In these figures, we plot the square root of the sum of the square of absolute values of the first and second components.

Self-consistent calculation of nonlinear band structures

To obtain the nonlinear band structures in Fig. 3, we numerically calculate the nonlinear eigenvalue problem by using the self-consistent method. We first rewrite the nonlinear dynamics as $i\partial_t \Psi = f(\Psi) = H(\Psi)\Psi$, where $H(\Psi)$ is a state-dependent effective Hamiltonian. Then, we conduct the self-consistent calculation in the following procedure. (1) We numerically diagonalize $H(\mathbf{0})$ and set the initial guess of the eigenvalue and eigenvector Ψ_0 and E_0, respectively, by adopting a pair of the obtained eigenvalue and eigenvector of $H(\mathbf{0})$. We fix the norm of Ψ_0 to be $||\Psi_0||^2 = wL$, where L is the system size. (2) We substitute the guessed eigenvector Ψ_i after i iterations into $H(\Psi)$ and diagonalize $H(\Psi_i)$. (3) We choose the obtained eigenvalue that is the closest to the previous guess E_i, and the corresponding eigenvector as the next guess E_{i+1} and Ψ_{i+1}. (4) We iterate steps (2) and (3) until the distance between Ψ_i and Ψ_{i+1} becomes smaller than the threshold of $||\Psi_{i+1} - \Psi_i|| < \epsilon$, or the iteration reaches a fixed number. We also perform these calculations starting from all the eigenvectors of $H(\mathbf{0})$ and obtain a set of nonlinear eigenvectors and eigenvalues of $f(\Psi)$.

In Fig. 3, we consider the parametrized state-dependent Hamiltonian that corresponds to the nonlinear Chern insulator under the assumptions of the y-periodic Bloch ansatz and the open boundary condition in the x direction. The state-dependent Hamiltonian is described as

$H(\Psi) =$

$$\begin{pmatrix} u + \Delta_x^2 + \cos k_y + \kappa\left(|\Psi_1|^2 + |\Psi_2|^2\right) & \left(i\Delta_x + i\sin k_y\right) \\ \left(i\Delta_x - i\sin k_y\right) & -\left(u + \Delta_x^2 + \cos k_y + \kappa\left(|\Psi_1|^2 + |\Psi_2|^2\right)\right) \end{pmatrix},$$

$$(23)$$

where Δ_x and Δ_x^2 are the difference operators defined as $\Delta_x \Psi(x) = [\Psi(x + 1) - \Psi(x)]/2$ and $\Delta_x^2 \Psi(x) = \Psi(x + 1) + \Psi(x - 1) - 2\Psi(x)$, respectively. Then, we calculate the nonlinear eigenvalues of this state-dependent Hamiltonian at $k_y = n\Delta k$, where $n = -N, -N+1 \ldots N-1, N$, and $\Delta k = \pi/N$ ($N = 50$). Here we set the system size in the x direction as $L = 10$ and fix the average amplitude of the nonlinear eigenvector as $\sum_{x,j} |\Psi_j(x; k_y)|^2/L = w$ independent of wavenumber k_y. We note that the self-consistent calculation is only stable at weak nonlinearity. To calculate the band structures in strongly nonlinear systems than those

analysed in the main text, one should instead use the Newton method (Supplementary Methods).

Theorem of bulk–boundary correspondence in weakly nonlinear systems

We mathematically show the bulk–boundary correspondence in weakly nonlinear systems. Here we use a simple notation $f(\Psi) = E\Psi$ instead of $f_j(\Psi; \mathbf{r}) = E\Psi_j(\mathbf{r})$, where Ψ is the nonlinear eigenvector whose components correspond to the state variables at locations $\mathbf{r}$ and internal degrees of freedom j. The claim of the theorem is as follows:

Theorem. Suppose $f(\Psi) = E\Psi$ is a nonlinear eigenvalue problem on a two-dimensional lattice system that satisfies the following assumptions. (1) When we rewrite the nonlinear function f as $f(\Psi) = H(\Psi)\Psi$, there exists a positive real number $c < 1$ that satisfies $||H(\Psi) - H(\mathbf{0})|| < gc/2$ for any complex vector Ψ, where g is the bandgap of $H(\mathbf{0})$ and $||\cdot||$ is the operator norm. (2) There exists a positive real number $c' < 1$ such that for any pairs of complex vectors Ψ and $\Psi + \Delta\Psi$ with the norm w, they satisfy $||H(\Psi + \Delta\Psi) - H(\Psi)|| \leq g(1-c)c'(6\sqrt{2}w)^{-1}||\Delta\Psi||$. (3) For any complex vector Ψ, one can rewrite the nonlinear function $f(\Psi)$ as $f(\Psi) = \tilde{H}(\Psi)\Psi$, where $\tilde{H}$ is a Hermitian matrix. (4) The nonlinear equation satisfies the $U(1)$ symmetry, $f(e^{i\theta}\Psi) = e^{i\theta}f(\Psi)$. We also assume that the number of nonlinear eigenvectors is equal to that of the linear eigenvectors of $H(\mathbf{0})$. Then, the nonlinear eigenequation $f(\Psi) = E\Psi$ exhibits robust gapless boundary modes if and only if its nonlinear Chern number is non-zero.

We note that here we relate the average amplitude $w_{\text{ave}} = \sum_{\mathbf{r},j} |\Psi_j(\mathbf{r})|^2/L$ to the amplitude used in the definition of the nonlinear Chern number. To prove the theorem, we first show the following proposition.

Proposition 1. In the nonlinear eigenvalue problem that satisfies the assumptions in the theorem, the self-consistent calculation converges, namely, $E_i \to E_\infty$ and $\Psi_i \to \Psi_\infty$. Furthermore, there exists an eigenvector Ψ_0 and eigenvalue E_0 of $H(\mathbf{0})$ that satisfy $||E_\infty - E_0|| < gc/2(1 - c')$ and $||\Psi_\infty - \Psi_0|| < 2^{-1/2}c(1 - 2c')^{-1}w$.

To show this proposition, we utilize the perturbation theorem of the eigenvectors in linear systems. Suppose H is a non-degenerate Hermitian matrix and g is the minimum difference between its two eigenvalues. If $||A|| < g/2$ in terms of the operator norm, for an arbitrary eigenvector Ψ of $H + A$, there exists an eigenvector Ψ_0 of H that satisfies $||\Psi - \Psi_0|| \leq Dg^{-1}||A||\,||\Psi_0||$ $(D = 2\sqrt{2})$. We iteratively use this theorem and evaluate the distance between the guess of eigenvectors Ψ_i and Ψ_{i+1} at each step.

We also show that the resulting eigenvalue and eigenvector, namely, E_∞ and Ψ_∞, respectively, are indeed a pair of nonlinear eigenvalue and eigenvector of $f(\Psi)$, which is summarized below.

Proposition 2. The converged solutions of the self-consistent calculation E_∞ and Ψ_∞ satisfy $f(\Psi_\infty) = E_\infty \Psi_\infty$.

We show this proposition by using simple inequalities and limit evaluations. By using these propositions, we finally show the following lemma to prove the theorem.

Lemma. For an arbitrary eigenvector of a nonlinear eigenvalue problem $(H + f(\Psi))\Psi = E\Psi$ that satisfies the conditions in the theorem, there exists the eigenvector of $[H + (1 - \epsilon)f(\Psi_\epsilon)]\Psi_\epsilon = E\Psi_\epsilon$ that satisfies $||\Psi - \Psi_\epsilon|| < Cw\epsilon$ ($0 < \epsilon < g'/g$, where g' is the minimum difference of the eigenvalues of $H + f(\Psi)$), where w is the norm of Ψ and Ψ_ϵ and C is a constant independent of the eigenvector Ψ and constant ϵ.

This lemma indicates that in weakly nonlinear systems, one can map the nonlinear eigenvalues and eigenvectors onto those of a linear eigenvalue problem. Thus, we can show the bulk–boundary correspondence in weakly nonlinear systems.

Derivation of the nonlinear Dirac Hamiltonian and its gapless mode

We have derived the nonlinear Dirac Hamiltonian (equation (25)) as the effective theory of the low-energy dispersion of the nonlinear QWZ model around the critical amplitude. For example, if we focus on the critical amplitude $w_c = (-2 - u)/\kappa$, the nonlinear band structure of the model closes the gap at $(k_x, k_y) = (0, 0)$. Then, around the critical amplitude $w \approx w_c$ and the gap-closing point $(k_x, k_y) \approx (0, 0)$, w remains the leading order term of the wavenumber-space description of the nonlinear QWZ model. Finally, by substituting the wavenumbers with the derivative, we derive the real-space description of the nonlinear Dirac Hamiltonian in equation (25) as

$$i\partial_t \Psi(\mathbf{r}) = \hat{H}(\Psi(\mathbf{r}))\Psi(\mathbf{r}), \tag{24}$$

$$\hat{H}(\Psi(\mathbf{r})) = \begin{pmatrix} m + \kappa\left(|\Psi_1(\mathbf{r})|^2 + |\Psi_2(\mathbf{r})|^2\right) & -i\partial_x + \partial_y \\ -i\partial_x - \partial_y & -m - \kappa\left(|\Psi_1(\mathbf{r})|^2 + |\Psi_2(\mathbf{r})|^2\right) \end{pmatrix}. \tag{25}$$

Starting from other critical amplitudes $w_c = -u/\kappa$ and $w_c = (2 - u)/\kappa$, one can derive similar state-dependent Hamiltonians (Supplementary Note 8).

We have also analytically calculated the spatial distribution of the gapless modes of the nonlinear Dirac Hamiltonian. Here we assume the Bloch ansatz $\Psi_i(x, y) = e^{ik_y y}\Psi_i'(x)$ that is periodic in the y direction and consider the semi-infinite system that has an open boundary at $x = 0$ and is extended to $x \to \infty$. We calculate the localized mode with the wavenumber k_y and the eigenvector $E = k_y$. Constructing an analogy to the linear case, one can use an ansatz $(\Psi_1(x, y), \Psi_2(x, y))^T = e^{ik_y y}\phi(x)(1/\sqrt{2}, -i/\sqrt{2})^T$ to describe the localized mode. Then, $\phi(x)$ should satisfy $\partial_x \phi(x) = m\phi(x) + \kappa|\phi(x)|^2\phi(x)$. We can analytically obtain the solution of this equation as

$$\phi(x) = e^{i\theta}\sqrt{\frac{1}{-(\kappa/m) + De^{-2mx}}}, \tag{26}$$

where D is the integral constant and $-(\kappa/m) + De^{-2mx}$ must be positive.

Nonlinear Chern number of the nonlinear Dirac Hamiltonian

To calculate the nonlinear Chern number of the nonlinear Dirac Hamiltonian (equation (25)), we use the Bloch ansatz $\Psi_i(x, y) = \psi_i(\mathbf{k})\exp(i(k_x x + k_y y))$ (without explicit (x, y) dependence because of the continuous translational symmetry). Then, we analytically obtain the nonlinear Chern number of the nonlinear Dirac Hamiltonian as

$$C_{NL} = \begin{cases} \frac{1}{2} & (m + \kappa w > 0) \\ -\frac{1}{2} & (m + \kappa w < 0) \end{cases}, \tag{27}$$

where $w = \int_S dS[|\Psi_1(x, y)|^2 + |\Psi_2(x, y)|^2]/|S|$ is the average squared amplitude of plane waves in this nonlinear system. We note that the nonlinear Chern number of the nonlinear QWZ model corresponds to the sum of those of the nonlinear Dirac Hamiltonians obtained from the expansion around the gap-closing points $(k_x, k_y) = (0, 0)$, $(0, \pi)$, $(\pi, 0)$, (π, π).

Numerical calculations of the quench dynamics

We have numerically solved the nonlinear Schrödinger equation (equation (15)) with the initial condition localized at the left edge (Fig. 5a). As the initial conditions, we study the two cases. One is

$$\Psi_1(x, y) = \delta_{x,1}/\sqrt{2}, \qquad \Psi_2(x, y) = i\delta_{x,1}/\sqrt{2}, \tag{28}$$

which corresponds to the solution with $u = -1$ of the linear model ($\kappa = 0$). The other is

$$\Psi_1(x, y) = (-1)^y \delta_{x,1}/\sqrt{2}, \qquad \Psi_2(x, y) = i(-1)^y \delta_{x,1}/\sqrt{2}, \tag{29}$$

which corresponds to the solution with $u = 1$ of the linear model ($\kappa = 0$). Supplementary Note 13 shows the derivation. For the numerical calculation, we used the NDSolve function in Mathematica (version 13.3). We consider a $L \times L$ lattice (we set $L = 10$ in the numerical calculation) under the open boundary condition in the x direction and the periodic boundary condition in the y direction.

We solve the nonlinear Schrödinger equation (equation (15)) under the two initial conditions in equations (28) and (29). The time evolution of $|\Psi_1(x, y)|^2 + |\Psi_2(x, y)|^2$ is shown in Fig. 5d,e. We define the phase indicator P as

$$P \equiv \max_{0.99T < t < T} \frac{1}{L} \sum_{y=1}^{L} \left[|\Psi_1(x = 1, y)|^2 + |\Psi_2(x = 1, y)|^2 \right], \tag{30}$$

where $T = 10$. We have $P \approx 0$ in the trivial phase (Fig. 5b), which implies the absence of localized edge states. On the other hand, we have $P \approx 1$ in a topological phase (Fig. 5c), which implies the presence of a localized edge mode. To elucidate the topological phase diagram, we plot P in the u–κw plane (Fig. 5d,e). We find that the phase indicator is 1 along the blue line, where the exact solution is valid. It shows that the exact solution is realized by the quench dynamics.

To compare the phase boundary obtained from the quench dynamics and the nonlinear Chern number, we relate the bulk amplitude w with the edge amplitude $w_{edge} = 1$. Then, grey lines in Fig. 5 show the phase boundary of the nonlinear Chern number. This definition of the amplitude under the open boundary condition is different from that used in the calculation of the nonlinear band structures because we should choose the proper definition to observe the bulk–boundary correspondence in each numerical method for demonstrating the nonlinear edge modes (Supplementary Methods).

Data availability
All relevant data to interpret the results of this study are included in the figures. All other data that support the plots within this paper and other findings of this study are available from the corresponding author upon reasonable request.

Author contributions
K.S., M.E., Y.A., N.Y. and T.S. planned the project. K.S. and M.E. performed the analytical and numerical calculations. K.S., M.E., Y.A., N.Y. and T.S. analysed and interpreted the results and wrote the paper.

Competing interests
The authors declare no competing interests.

Additional information